

CO₂ capture by novel hierarchical activated ordered micro-mesoporous carbons derived from low value coal tar products

Citation for published version:

García-Díez, E, Castro-Muñiz, A, Paredes, JI, Maroto-Valer, MM, Suárez-García, F & García, S 2021, 'CO₂ capture by novel hierarchical activated ordered micro-mesoporous carbons derived from low value coal tar² products', *Microporous and Mesoporous Materials*, vol. 318, 110986.
<https://doi.org/10.1016/j.micromeso.2021.110986>

Digital Object Identifier (DOI):

[10.1016/j.micromeso.2021.110986](https://doi.org/10.1016/j.micromeso.2021.110986)

Link:

[Link to publication record in Heriot-Watt Research Portal](#)

Document Version:

Peer reviewed version

Published In:

Microporous and Mesoporous Materials

Publisher Rights Statement:

© 2021 Elsevier Inc.

General rights

Copyright for the publications made accessible via Heriot-Watt Research Portal is retained by the author(s) and / or other copyright owners and it is a condition of accessing these publications that users recognise and abide by the legal requirements associated with these rights.

Take down policy

Heriot-Watt University has made every reasonable effort to ensure that the content in Heriot-Watt Research Portal complies with UK legislation. If you believe that the public display of this file breaches copyright please contact open.access@hw.ac.uk providing details, and we will remove access to the work immediately and investigate your claim.

CO₂ capture by novel hierarchical activated ordered micro-mesoporous carbons derived from low value coal tar products

Enrique García-Díez^a, Alberto Castro-Muñiz^b, Juan Ignacio Paredes^b, M. Mercedes Maroto-Valer^a, Fabián Suárez-García^{b}, Susana García^{a*}*

^aResearch Centre for Carbon Solutions (RCCS), School of Engineering and Physical Sciences, Heriot-Watt University, Edinburgh EH14 4AS, United Kingdom

^bInstituto de Ciencia y Tecnología del Carbono, INCAR-CSIC, C/Francisco Pintado Fe 26, 33011, Oviedo, Spain.

*E-mail address: fabian@incarcsic.es (Fabian Suárez-García).

*E-mail address: s.garcia@hw.ac.uk (Susana García).

ABSTRACT

Activated ordered mesoporous carbon (AOMC) sorbents for CO₂ capture have been synthesized, characterized and evaluated. They were obtained using low-value products from the distillation of coal tar and following a hard templating method to achieve an ordered mesoporous structure. Both physical and chemical activation processes were applied. It was observed that neither physical nor

chemical activation affected the mesopore structure of the samples. Regarding the CO₂ capture, the best chemical AOMC was the one activated at 850 °C with a KOH:carbon ratio of 4:1 (2.48 mmol/g AOMC), whilst the best physical activated one was obtained upon activation during 48 h with a burn-off degree of 48% and dissolving the template afterwards (2.38 mmol/g AOMC). In the present case the ordered mesoporous structure was thought to facilitate CO₂ diffusion into the micropores of the porous carbons. The best samples were tested for CO₂ capture at different operational conditions, considering capture temperatures up to 150 °C and CO₂ partial pressures between 5 and 90 % (balance N₂). Their performance was also tested over six adsorption-desorption cycles, and it was determined that the working capacity remained constant and the mesoporous structure was not modified.

KEYWORDS: Ordered Activated Carbon, Coal Tar products, CO₂ capture, Adsorption, Mesopore structure

1. Introduction

To reach the temperature rise limitation of the planet to 1.5 °C set in the Paris Agreement, different actions have to be taken. Amongst them, the use of carbon capture and storage (CCS) technologies is one of the most relevant to reduce the CO₂ emissions into the atmosphere¹. Nowadays, the most advanced carbon capture technology involves the absorption of CO₂ by amines. However, it suffers from important problems of stability against corrosion and high energy requirements for the regeneration process. For this reason, the use of solid sorbents is becoming more relevant as less energy for CO₂ desorption is needed and the adsorbents are more corrosion-stable²⁻⁴ than liquid absorbents.

Depending on the CO₂ capture temperature, solid adsorbents can be classified into three different groups: low- (< 200 °C), intermediate- (200-400 °C) and high-temperature (> 400 °C). For low temperature adsorbents, zeolites, ordered mesoporous silica, metal-organic frameworks (MOFs), porous organic polymers (POPs) and activated carbons (ACs) have been already evaluated for CO₂ physical adsorption ^{4,5}, which is associated with low costs in the capture-desorption process ⁶. Furthermore, ACs show great promise as solid adsorbents due to their high stability through cycles, low cost and easy production, as well as high surface area, which are required characteristics for a high CO₂ capture capacity ^{7,8}. However, in spite of these promising characteristics, the main disadvantage of using ACs for CO₂ capture is that they usually present a randomly distributed pore network with intricate paths that inhibit the diffusion of the CO₂ molecules ⁸.

As it has been reported previously, the CO₂ capture capacity at atmospheric pressure is directly related to the micropore volume, as CO₂ adsorption mainly takes place in the narrow pores of the material (< 2nm) ^{5,9,10} at temperatures ≤ 25 °C. On the other hand, at higher temperatures the overall surface area of the adsorbent becomes more relevant ¹¹. However, as Vorokhta et al. ¹² and Song et al. ¹³ concluded, the CO₂ adsorption capacity of the material above atmospheric pressure is also dependent on the mesopore volume. Even more, it was found that under pre-combustion operational conditions (pressures up to 40 bar), mesoporous carbons exhibited a higher CO₂ capture capacity than that of commercial ones with a higher micropore volume, as well as lower energy requirements for the regeneration process. Li and Xiao evaluated the CO₂ capture behavior of a dual pore AC, reaching values similar to those of commercial ACs at 25 °C and 1 atm. It was concluded that the presence of mesopores facilitate access of the CO₂ molecules to the main adsorption sites at the micropores ¹⁴. For this reason, a useful strategy to increase the CO₂ capture

capacity of porous carbons is to increase the micropore volume of the carbon while retaining a considerable mesopore structure.

On this regard, Lou et al.¹⁵ reported a capture capacity of 8.1 mmol of CO₂ per gram of sample at 1 bar and 0 °C using polymer based N-doped activated carbon polymer with a high microporosity. On the other hand, Mane et al.¹⁶ evaluated hierarchical porous N-doped polymers materials for CO₂ capture. They obtained a capture capacity of 2.23 mmol of CO₂ /g at 25 °C and 1 bar which was increased up to 4.52 mmol of CO₂/g at 0 °C and 1 bar. Zabiegaj et al.¹⁷ evaluated carbon monoliths with a hierarchical pore structure, which gave a CO₂ capture of 2.62 mmol of CO₂/g at 25 °C and 1 bar.

ACs are produced by physical (also called thermal) or chemical activation of a carbon precursor, which can be coal¹⁸⁻²¹, a pyrolyzed organic material²²⁻²⁵, or biomass²⁶⁻³⁰. Physical or thermal activation consists of the oxidation of the carbon sample with CO₂ or water at temperatures higher than 800 °C³¹. On the other hand, chemical activation proceeds through impregnation of the organic precursor itself (one step) or the organic precursor after pyrolysis (two steps) with an activating agent (typically KOH), followed by heating at temperatures commonly lower than the ones required for physical activation⁴. The objective of these activation processes is to attain higher surface areas and pore volumes, specifically micropore volumes. However, it is very difficult to control independently the micropore and mesopore structures with these conventional methods. To control more accurately the porosity of carbon materials, the hard-templating method has been developed³²⁻³⁴. Hard-templated carbons are usually obtained by infiltration of a carbon precursor into the pore network of an inorganic porous solid (template), the porous structure of which is easily controlled. After carbonization and removal of the template, a carbon material is obtained with a porosity that is a replica of that of the template. The porosity of the template

carbons can be further developed by subjecting them to the activation methods conventionally applied in the preparation of ACs ³⁵.

In this study, ordered mesoporous carbon (OMC) materials obtained from creosote, a low-value coal tar distillation product used as a carbon precursor by a recently reported method ³⁶, were modified by physical and chemical activation. These activated ordered mesoporous carbons (AOMCs) were tested under post-combustion operational temperatures. Different CO₂ partial pressures, between 5 and 90 vol.%, were considered to evaluate the CO₂ capture uptakes of the different carbons simulating different flue gas conditions ^{37, 38}. Finally, the best physical and chemical activated carbons were tested under different desorption temperatures (125-200 °C) and atmospheric pressure over several adsorption-desorption cycles, and the stability of their ordered mesoporous structure was evaluated.

2. Material and methods

2.1 Ordered mesoporous carbon preparation

Ordered mesoporous carbon materials were prepared following the hard templating method. SBA-15 was used as an ordered mesoporous silica (OMS) template and creosote, a low-value coal tar distillate, as the carbon precursor (See Scheme 1) and the followed methodology is described elsewhere ³⁶.

SBA-15 was synthesized following the methodology described elsewhere ³⁹. Detailed preparation is described in ³⁶. Briefly, the non-ionic triblock copolymer surfactant Pluronic P123 (Mw = 5800, Aldrich) was dissolved in a solution of HCl (Merck, 37 wt%) in water by stirring the mixture for 24 h at 40 °C. Then, tetraethoxysilane (Aldrich 98.6% ACS reagent) was added and the mixture was further stirred for 4 h. Next, the solution was transferred to a 750 ml autoclave to age the silica

precursor material at 110 °C for 72 h. The mixture was subsequently filtered, thoroughly washed with both distilled water and ethanol, and dried at 80 °C overnight. Finally, the surfactant was removed by calcination at 550 °C for 6 h.

Infiltration of the template with the carbon precursor was carried out as follows: the creosote (supplied by the company Bilbaína de Alquitranes S.A., Spain) was mixed with sulphuric acid (Sigma 95-98% ACS reagent) in a ratio creosote:H₂SO₄ 9:1 vol./vol., and the mixture was kept at 40 °C overnight. Two phases were formed, a viscous one at the bottom and a more liquid one at the top. The viscous part was separated and put in contact with the SBA-15 template in a round-bottom flask. The temperature was raised to 110 °C under vacuum, and then the flask was pressurized with argon (minimum purity 99.9990%). The pressure was kept slightly over atmospheric pressure for 2 h.

The resulting OMS/carbon precursor composite was heat treated in a horizontal furnace at 950 °C under an argon flow (minimum purity 99.9990%; heating rate: 1 °C/min; flow rate: 500 ml/min) to obtain an OMS/carbon composite with a 37.9 wt.% of carbon. The carbon material was released from the template by washing the composite with 1 M NaOH solution at 40 °C for 24 h, a much milder alternative to the use of HF solutions as the etchant and it has shown their effectiveness in previous work^{40, 41}. Here, silica is dissolved at pH values above 9 through the hydrolysis of Si-O-Si bonds as $\text{SiO}_2(\text{s}) + 2\text{H}_2\text{O} \rightleftharpoons \text{Si}(\text{OH})_4$ ⁴². The resulting silicic acid is released into the aqueous phase and it can be dissociated into different silicates such as $\text{Si}(\text{OH})_4 + \text{OH}^- \rightleftharpoons (\text{HO})_3\text{SiO}^- + \text{H}_2\text{O}$ ⁴³. Furthermore, by deploying NaOH as the etchant the resulting silicates can be readily reused to synthesize the template again, thus optimizing the utilization of precursors and minimizing the generation of waste. Finally, the carbon was washed with water in a Soxhlet apparatus until the

washing liquids reached conductivity values lower than 3 $\mu\text{S}/\text{cm}$ and dried under vacuum at 110 $^{\circ}\text{C}$ for 12 h. The resulting carbon material was denoted as OMC_{Creo} (see Scheme 1, path I).

2.2 OMC porosity modification

The porosity of the obtained carbon materials was further developed through subsequent physical and chemical activation protocols specifically designed for OMCs, as described elsewhere^{44,45} and detailed in the following.

2.2.1 Chemical activation of the OMCs

The OMS/carbon composite was mixed with KOH at different KOH to carbon ratios (XKOH=1:1, 2:1, 3:1 and 4:1). The amount of carbon in the OMS/carbon composite was estimated by using thermogravimetric analysis from the weight loss after the combustion of the sample in air at 850 $^{\circ}\text{C}$ for 1 h. The KOH and OMS/carbon composite mixture was then heated up to the activation temperature (TA = 650 $^{\circ}\text{C}$, 750 $^{\circ}\text{C}$ and 850 $^{\circ}\text{C}$; heating rate: 10 $^{\circ}\text{C}/\text{min}$) under inert atmosphere (Ar, minimum purity 99.9990%, flow rate: 250 ml/min) in a horizontal tubular furnace (60 mm inner diameter) and kept for one hour at that temperature. When room temperature was reached, the samples were placed in a 1 M HCl solution and kept under stirring for 2 hours, in order to remove alkali metals and non-reacted KOH. Then, the activated composites were recovered by filtration and extensively washed with hot water. Finally, the remaining silica was dissolved with NaOH as indicated in section 2.1. The samples were denoted as OMC_{Creo} CA XKOH TA (see Scheme 1, path II).

2.2.2 Physical activation of the OMCs

Two different approaches were taken to modify the preparation of the OMCs by the gasification of the materials with CO₂. On one side, the OMC_{Creo} was heat-treated under inert atmosphere (Ar,

minimum purity 99.9990%, flow rate: 250 ml/min) up to 800 °C (heating rate: 10 °C/min) in a horizontal tubular furnace (60 mm inner diameter). Then, the gas was switched to CO₂ for different activation times (t_A) to obtain materials with different burn-off degrees (BO). These samples were named as OMCreo PAc BO (see Scheme 1, path III). The other set of samples was obtained by the physical activation of the OMS/carbon composite under the same conditions as before, and the silica template was dissolved afterwards. The BO degree was calculated from the amount of carbon in the composite before and after the activation step using thermogravimetric analysis as described before. These samples were denoted as OMCreo PAt BO (see Scheme 1, path IV).

2.3 Characterization of materials

The amount of material infiltrated in the silica template and the amount of silica that remained after activation processes and etching with NaOH in the activated carbons was estimated in a thermobalance (SDT Q600 from TA Instruments) from the weight loss after the combustion of the sample in air (minimum purity 99.998 %, flow rate: 50 ml/min) at 850 °C for 1 h. Elemental analyses were performed in a LECO CHNS-932 microanalyser. The nanometre-scale morphology and structure of the materials were analysed with transmission electron microscopy (TEM; 2000 EX-II from JEOL, at an acceleration voltage of 160 kV) and X-ray diffraction (XRD; D5000 diffractometer from Siemens, with 0.01°/step and 2 s/step, source slit: 0.2 mm and detector slit: 0.6 mm), respectively. Raman spectroscopy was performed with a LabRam instrument (Horiba Jobin–Yvon) using a 532 nm wavelength laser at a low incident power (0.5 mW) to avoid altering the samples. The porous texture of the materials was probed by physical adsorption/desorption of N₂ at -196 °C and CO₂ at 0 °C, in a volumetric analyser (Autosorb-1 from Quantachrome). The samples were degassed at 150 °C under vacuum for 15 h prior to the measurements. The surface area, S_{BET} , was calculated by the Brunnauer-

Emmet-Teller (BET) equation ⁴⁶ from the N₂ adsorption data in the relative pressure range of ca. 0.01 ~ 0.2 and the total pore volume, V_T, was obtained by the Gurvich rule from the amount of adsorbed N₂ at a relative pressure of 0.9. The micropore volume, V_{DR, N₂}, was calculated by applying the Dubinin-Radushkevich method ⁴⁷ to the N₂ adsorption isotherms, and the mesopore volume, V_{mp}, was estimated as V_{mp}=V_T – V_{DR, N₂}. The micropore volume from the narrowest microporosity was obtained by applying the Dubinin-Radushkevich method to the CO₂ adsorption isotherms, V_{DR, CO₂}. The pore size (dp) distribution (PSD) of the samples was calculated by applying the non-local density functional theory (NLDF) in the quenched solid density functional theory (QSDFT) method developed by Quantachrome ⁴⁸ to the N₂ adsorption branch using the QSDFT equilibrium model. Due to the well-known diffusional problems in pores with sizes < 0.5 nm that N₂ at -196 °C has, the complementary use of CO₂ at 0 °C is recommended ^{49, 50}. Thus, the higher adsorption temperature results in a faster diffusion in the narrowest micropores. However, due to the high saturation pressure of CO₂ at 0 °C, a p/p₀ of only 0.03 can be reached limiting the characterization to the narrow micropores. Thus, V_{DR, CO₂} is the volume of narrow micropores (from about 0.34 to 0.7 – 0.8 nm) and V_{DR, N₂} is the micropore volume from about 0.5 to 2 nm.

2.4 CO₂ capture uptake evaluation

The CO₂ capture capacities were determined using a thermogravimetric analyser TAQ500 (TA Instruments). In all the experiments, 10 mg of sample were placed in a platinum pan and heated to 120 °C at 10 °C/min and under 100 ml/min of N₂ to dry and desorb any pre-adsorbed gases on the surface of the sample. After drying and cooling under N₂ down to 25 °C, the sample was kept under N₂ flow until a constant weight was reached. Then, the gas is switched

to a 90% CO₂ gas stream (100 ml/min of total flow, balance N₂) and maintained for 30 minutes.

For the best performing physical and chemical AOMCs, different capture temperatures were tested (50-150 °C), and isotherms were obtained at 25 °C under different CO₂ concentrations, from 5 to 90 vol.% (balanced with N₂). CO₂ partial pressures from 5 to 30 vol.% simulate common CO₂ concentrations in natural gas, pulverized coal combustion and cement plants flue and off-gasses^{37, 38}. Next, the stability of the best samples was evaluated after six adsorption-desorption cycles, under different regeneration temperatures (i.e., 125, 150, 175 or 200 °C) and at a constant adsorption temperature of 25 °C. Moreover, a thermostability study of the best samples was carried out, to determine the behaviour of the samples from 25 to 220 °C with a heating ramp of 10 °C/min under 100 ml/min of pure N₂.

3. Results and discussion

3.1 Physicochemical characterization

3.1.1 Textural characterization

The effect of temperature on the chemical activation with KOH was studied by fixing the X_{KOH} ratio to 4:1 and heating the mixture of KOH and OMS/carbon composite at different temperatures (650, 750 and 850 °C). All of the OMC_{Creo} CA 4:1 T_A samples showed complex isotherms that could be classified as a combination of type I(b) at low relative pressures, type IV(a) at intermedium p/p₀ and type II at p/p₀ > 0.9. The hysteresis loop change from H2(a) for non-activated sample (OMC_{Creo}) to H2(b) for the activated ones (see Figure 1a), which is typical of mesoporous materials with a complex porous texture⁴⁹⁻⁵¹. The increase in the N₂ uptake above 0.9 can be due to inter-particle N₂ condensation and not to the presence of wide

mesopores or macropores. These samples are mainly constituted of submicrometric particles as showed in TEM images (see Figures 5, SI2 and SI4) and the presence of wide mesopores or macropores were not observed. Thus, the total pore volume, V_T , was calculated at $p/p_0=0.9$, where the conditions for applying the Gurvich rule are valid.

It is noteworthy that the microporosity ($< 2\text{nm}$) of the samples (Figure 1) was not affected at an activation temperature of $650\text{ }^\circ\text{C}$ as the low-pressure region ($p/p_0<0.4$) of the N_2 adsorption isotherms as well as the CO_2 adsorption isotherms of OMCreo and OMCreo CA 4:1 $650\text{ }^\circ\text{C}$ (see Figure 1a and Figure 1b) were very similar. The micropore volume $V_{\text{DR}, \text{N}_2}$ rapidly increased with the activation temperature from 650 to $850\text{ }^\circ\text{C}$ (see Table 1).

Regarding the narrow microporosity (pores sizes $< 0.7 - 0.8\text{ nm}$), both $V_{\text{DR}, \text{CO}_2}$ and pore size, increased with the activation temperature (see Table 1 and Figure 1d). The pore size distributions calculated from the CO_2 adsorption isotherms exhibited three peaks: at pore sizes lower than 0.4 nm , between 0.4 and 0.7 nm and the last one with the maxima at 0.8 nm . The minimum at 0.4 nm might be due to an artifact of the DFT method ⁵², but, even if this is considered, the effect of the activation temperature can be observed: the volume of narrow micropores, especially for pores $< 0.4\text{ nm}$, increased for sample prepared at $750\text{ }^\circ\text{C}$, and at higher activation temperature (i.e. $850\text{ }^\circ\text{C}$) the contribution of micropores of 0.6 nm become more important.

The effect of the KOH ratio was studied by keeping the activation temperature at $850\text{ }^\circ\text{C}$ while changing the KOH to carbon ratio ($X_{\text{KOH}}=1:1, 2:1, 3:1$ and $4:1$). All of the samples showed again complex isotherms formed by type I(b) at low relative pressures, type IV(a) at intermedium p/p_0 and type II at $p/p_0> 0.9$. Similar evolution of the hysteresis loop from H2(a) for non-activated sample (OMCreo) to H2(b) when X_{KOH} increased up to $4:1$ was observed

(see Figure 2a). All the textural parameters (S_{BET} , $V_{\text{DR, N}_2}$ and $V_{\text{DR, CO}_2}$), except V_T , gradually increased as X_{KOH} increased (see Table 1).

The impregnation ratio, X_{KOH} , does not affect the pore size distributions for $X_{\text{KOH}} < 3:1$ and only an increase in the volume of micropores < 0.4 nm was observed (see Figure 2d). Only for sample prepared at $X_{\text{KOH}}=4:1$ a widening of the narrow microporosity (pores sizes $< 0.7 - 0.8$ nm) is observed in the PSD. Thus, it is observed a decrease in the contribution of pores < 0.4 nm and an increase for pores between 0.4 and 0.7 nm in the PSD from CO_2 (Figure 2d) and especially for pores at 0.9 nm, as seen in the PSD from N_2 (Figure 2c).

All of the chemically activated samples showed a well-developed mesoporous structure, but both the activation temperature and the KOH to carbon ratio caused a shift of the PSDs to lower pore sizes in the mesopore region (Figures 1c and 2c), probably due to a partial collapse of the OMC mesostructure upon activation.

The physical activation of the OMS/carbon composite and the OMCreo sample provided materials with similar $V_{\text{DR, N}_2}$ and $V_{\text{DR, CO}_2}$ volumes as in the case of the KOH activated ones (see Table 1). In this case, both micropore volumes, $V_{\text{DR, N}_2}$ and $V_{\text{DR, CO}_2}$, increased with the BO degree and also the micropore size distributions, either from N_2 and CO_2 isotherms (Figures 3c and d) became wider with this parameter. On the other hand, the mesopore volume was changed to a greater extent in this case (see Figure 3a), yielding higher V_{mp} values for the OMCreoPac BO (see Table 1).

The activation method (OMCreoPac vs. OMCreoPAT) had a strong influence on the PSDs of the materials in the mesopore region (see Figure 3c). The OMCreo Pac samples showed very narrow PSDs and very similar for BO=15% and 45%, while the one of the OMCreo PAT 48% widened significantly. In the case of the OMCreo PAT BO, the presence of the silica might

have hindered the CO₂ diffusion, and hence the activation of the sample. This would be translated to higher activation times needed to obtain similar BO degrees. Thus, the OMCreo PAc 45% was obtained with $t_A=24$ h while OMCreo PAt 48% required 48 h of activation. Additionally, this lower CO₂ diffusion could render a less homogenous activation, thus, the carbon atoms most exposed will be those that will be gasified to a greater extent.

3.1.2 Elemental analysis

The original OMC had a relatively high nitrogen and sulfur content (see Table SI1 in the Supplementary Information) that comes from the precursor and the H₂SO₄ used in the polymerization of creosote, respectively, as demonstrated previously⁵³. The latter was drastically reduced upon KOH activation, most probably due to the washing step with HCl that is thought to remove sulfur moieties. In the case of the nitrogen content, it decreases when the conditions of the chemical activation process become more extreme. Thus, the nitrogen content decrease with increasing activation temperature and impregnation ratio (i.e. amount of KOH). This indicates that the KOH reacts with the nitrogen surface groups favoring their elimination. On the other hand, both series of activated carbons prepared by physical activation (PAt and PAc series) have a N content between 2.87 and 2.97 wt.%, which is slightly lower than that of the non-activated sample (OMCreo). This small decrease may be due to the elimination of some of the nitrogen-containing groups due to the effect of thermal treatment. Activation of the OMS/carbon composite with KOH (CA series) and by physical activation (PAt series) rendered materials with a higher oxygen content than that present in the case of the OMC physical activation (PAc series). In the last preparation method, the gasification of the OMCreo sample with CO₂ did not affect the amount of oxygen-containing surface groups, but in the former two preparation methods (CA and PAt series) the removal

of the template with NaOH was carried out after the activation step, resulting in an oxidation of the carbon surface as it is indicated by the high oxygen content. The amount of silica that remained in the activated carbons was lower than 3 wt.% for CA and PAt series as determined by TG analysis. OMCreo sample had an ash content of 2.5 wt.%, similar to that for sample OMCreoPAc 15% (2.9 wt.%). OMCreo PAc 45% was the sample with the highest ash content (4.9 wt.%) due to the extensive gasification (BO of 45%) of sample OMCreo used as precursor in these series.

3.1.3 Raman analysis

The Raman spectra of OMCreo and the AOMCs (see Figure SI1 in the Supporting Information) exhibited two wide bands centered at ca. 1340 cm^{-1} (D band) and 1590 cm^{-1} (G band), typical of disordered carbons. The OMCreo sample showed a higher crystallinity than the AOMCs with an intensity ratio $I_D/I_G=0.90$. The AOMCs showed G bands with lower intensities than their corresponding D bands because the activation of the carbon materials introduced some defects in the carbon structure. Nevertheless, all the AOMCs show very similar I_D/I_G ratios with values between 1.00 and 1.08.

3.1.4 XRD analysis

The non-activated mesoporous carbon (OMCreo) showed a XRD pattern with a sharp peak at $2\theta = 0.90^\circ$ corresponding to the (1 0 0) reflection, and two weak peaks at $2\theta = 1.56^\circ$ and 1.80° assigned to the (1 1 0) and (2 0 0) reflections (see Figure 4).

The presence of those peaks indicated that the mesostructural order of the SBA-15 template was well reproduced in the resulting carbon (as a negative replica), as thus that the latter possessed a well ordered mesoporosity. The intensity of the (1 0 0) peak decreased and

widened with increasing activation temperature, but it was still present at 850 °C (see Figure 4a), suggesting that the mesoscale order of the samples was largely retained.

A similar behavior was observed in the case of chemical activation with different KOH to carbon ratios, i.e., the intensity of the (1 0 0) peak in the XRD patterns (see Figure 4b) tended to decrease and widen as the KOH to carbon ratio increased. However, even at the harshest conditions in this study (activation temperature: 850 °C; KOH:carbon=4:1), the porous carbon material still showed an ordered mesoporous structure. In the present chemical activation method which was, based on activating the OMS/carbon composite rather than the stand-alone carbon, the silica protected the thin carbon bars that connect the thick parallel ones (see Scheme 1) and prevent the collapse of the structure ⁴⁵. In the case of physical activation of OMCreo, the mesostructure of all of the samples was also retained even at the highest BO degrees (see Figure 4c). Interestingly, as shown in Figure 4 b and c, the activation of the OMCreo (PAc samples) gave rise to an OMC with a larger extent of mesostructural order than in the case of activation of the OMS/carbon composite (PAt samples). As discussed above, the activation of OMS/carbon composite required much longer activation times because the silica template probably blocked CO₂ gas diffusion into the carbon within the composite. Thus, activation might have taken place mainly in the outer part of the composite particles. Furthermore, the high activation temperature ($T_A=800$ °C) might have caused a contraction of the silica template ⁵⁴, resulting in damage to the carbon structure.

3.1.5 TEM analysis

The preservation of the mesoporous structure was confirmed by directly observing the nanostructure of the materials by TEM, as shown in Figure 5. All the samples showed the characteristic mesostructure of OMCs obtained with SBA-15 as a hard-template, i.e. an array

of mesochannels running parallel to the axis of the particles ⁵⁵, already observed for the OMCreo in our previous study ³⁶.

However, sample OMCreo CA 4:1 850 showed particles with a rough outer surface (see Figure 5b), probably because the silica template was completely dissolved in the outer part of the particles during activation, and therefore the carbon structure was more affected in that area. As for the physically activated materials, the OMCreo PAt 48% sample showed also a less ordered mesostructure at the surface of the particles (see Figure 5d) than that of the OMCreo PAc 45% (see Figure 5c). This observation suggested that the presence of the silica template made the activation step less homogeneous, giving rise to materials with wider PSDs, as indicated previously. In the case of the samples having the least damaged surface, e.g. OMCreo CA 1:1 850 and OMCreo PAc 45%, it was even possible to clearly observe the hexagonal array of solid carbon cylinders from the top of the particles, as seen in Figure SI2 in the Supporting Information.

3.2. CO₂ capture capacity

3.2.1. CO₂ capture capacity evaluation

Figure 6 shows the CO₂ capture uptake, in mmol of CO₂ per gram of AOMC, at 25 °C for each evaluated sample. It can be observed that both activation methods led to an increase in the CO₂ capture values, with a maximum value of 2.38 mmol of CO₂/g AOMC for the OMCreo CA 4:1 850 (chemically activated), followed by sample OMCreo Pat 48% with 2.18 mmol of CO₂/g AOMC (physically activated). These values are lower than those last reported using new carbon polymer-based samples N-doped with a high surface area and completely microporous ¹⁵. However, these values exceed previously reported capture capacities for mesoporous carbon-based materials and even for high microporous polymer-based carbons

^{12,16,56} and similar to capture capacities of hierarchical porous foam carbons ¹⁷. The capture capacities of the best samples reported here are also better than those previously reported for other non-carbon standard materials such as alumina, and silica gel. On the other hand, previously reported CO₂ capture values for zeolites, which show CO₂ capture capacities of 5 up to mmol/g at 25 °C ⁵⁷, and Metal Organic Frameworks ⁵⁸, exceed the values presented here. The advantage of ACs is that they are hydrophobic and CO₂ adsorption will be less negatively affected by the presence of water than in the case of zeolites and most MOFs.

The CO₂/N₂ selectivity values were calculated for these best activated carbons, and they have been compared with the non-activated material: OMCreo CA 4:1 850: 7.84; OMCreo Pat 48%: 5.96; OMCreo: 4.49. The obtained values are slightly lower than values previously reported, i.e.: 10-13 obtained from N-doped AC ⁵⁹ and Activated carbon foams ⁶⁰.

The abovementioned two samples with the highest capture capacity also showed the highest micropore volume percentage, but not the highest surface area and total pore volumes, which corroborates previous studies where the micropore volume was identified as the main factor for high CO₂ capture capacities ^{11,61}. In the CO₂ capture process, CO₂ diffuses through the ordered mesoporous channels to be adsorbed on the surface of the micropores ^{5,10}. The chemical activation with a higher X_{KOH} ratio and activation temperature and, the physical activation with the highest BO yielded a higher micropore volume, and as a consequence a higher CO₂ uptake for both activated carbons. It has to be highlighted that the elimination of the silica template afterwards seems to improve the CO₂ capture capacity. It can be observed that the sample OMCreo PAt 3% showed a higher CO₂ capture capacity than the sample OMCreo Pac 15%, having a lower BO. In all cases, it has been observed that a low BO gives a considerable increase of the CO₂ capture from the OMCreo not activated. This implies that,

even a low BO in the physical activation is enough to create micropores, also increasing the surface area, which helps in the CO₂ adsorption.

3.2.2. Effect of adsorption temperature and CO₂ partial pressure on CO₂ uptake

In post-combustion processes, the most common range for flue gas temperature is between 50 and 120 °C^{2,62}. When CO₂ adsorption by AOMCs is a physisorption process (an exothermic process), the CO₂ capture decreases as the temperature is increased. Figure 7 shows the CO₂ uptake for samples with the highest capture capacity at 25 °C, namely OMCreo PAt 48% and OMCreo CA 4:1 850.

As expected, the CO₂ capture capacities of both samples decreased as the adsorption temperature increased, and the OMCreo CA 4:1 850 sample exhibited, at any temperature, a higher CO₂ capture capacity than that shown by the physically AOMC, OMCreo Pat 48%. Although in a previous work, it was concluded that the surface area and the total pore volume become more important parameters for CO₂ adsorption at high temperatures¹¹, in the present case the sample with the lowest total pore volume but the highest micropore volume percentage boasted a higher CO₂ uptake. This result might be due to the well-ordered mesopore structure of the present carbon, which allows a better access of the CO₂ molecules to the micropore volume. The effect of different partial pressures of CO₂ in the gas stream was also evaluated here, as it largely differs amongst applications. For instance, it can take values between 5 and 30 vol.%, being the most common concentrations 8 and 15 vol.% in pulverized coal-fired plants³⁸, and 30 vol.% for cement plants³⁷.

As previously mentioned, the most important textural parameter is the micropore volume and its volume fraction, leading to higher CO₂ uptakes as these parameters increase. Furthermore, at low CO₂ concentrations, the narrow pores with sizes below 0.6 nm become more important

²¹. Figure 8 shows the CO₂ adsorption capacities at 25 °C for OMCreo CA 4:1 850 and OMCreo PAt 48% at different CO₂ partial pressures. It can be observed that for any CO₂ partial pressure the chemically activated OMCreo CA 4:1 850 sample outperformed its physically activated counterpart.

This highlights the importance of the narrow microporosity for CO₂ adsorption. Moreover, both samples showed a better CO₂ capture capacity under post-combustion operating conditions than commercial activated carbons ⁶³, and comparable to recently reported microporous activated carbons ⁶⁴. The obtained values are slightly lower than those obtained with other mesoporous carbons, which were doped with N₂ ⁶⁵.

3.2.3. CO₂ working capacity evaluation

In a CO₂ capture process, a key target is to evaluate the feasibility of the material in terms of its ability to endure a large number of adsorption-desorption cycles. In temperature swing adsorption (TSA) processes, CO₂ desorption is reached by heating the fully or partially saturated sample, which can have a negative effect on the structural stability and CO₂ capture capacity of the material upon cycling, i.e. its CO₂ working capacity. Figure 9 shows six adsorption-desorption cycles for samples OMCreo CA 4:1 850 and OMCreo PAt 48%, where the adsorption and desorption processes were evaluated at 25 and 200 °C, respectively.

A decrease in weight after desorption step can be observed. The thermostability of the samples, as the variation of weight with the increase of temperature is represented in Figure SI3. A decrease in weight associated with the elimination of moisture, followed by a slight decrease of weight until stabilization, can be noticed. This behavior suggests the possibility of a negative effect on the structure and stability of the sample, and as a consequence a decrease in the CO₂ working capacity, due to a high desorption temperature.

However, as it is shown in Figure 10, the CO₂ working capacity at 25 °C using different desorption temperatures (125, 150, 175 and 200 °C) remained unaltered through all cycles (2.37-2.39 mmol CO₂/g AOMC for OMCreo CA 4:1 850 and 2.15-2.2 mmol CO₂/g AOMC for the OMCreo PAt 48%).

This corroborates the stability of the samples upon cycling, even using a high temperature for the regeneration step. Furthermore, the mesoscale order as well as the porous texture remained unaltered after the working capacity tests as observed by TEM (see Figure SI4).

4. Conclusions

In this work, for the first time, a family of novel activated ordered mesoporous carbons have been synthesized from low value coal tar-derived products and evaluated for CO₂ capture under post-combustion operating conditions (adsorption temperature, CO₂ partial pressure). Two different modification routes were followed, physical and chemical activation. The best chemical activated sample, OMCreo CA 4:1 850 (with a CO₂ capture capacity of 2.38 mmol/g AOMC) and the best physical activated carbon, OMCreo PAt 48% (with a CO₂ capture capacity of 2.18 mmol/g AOMC, both at 25 °C and 90 vol.% of CO₂ in N₂). The activation procedure increased the micropore volume of the OMCs while retaining their well-ordered mesoporosity. It was observed that the mesostructural order enhanced the access of CO₂ to the narrow microporosity, giving rise to CO₂ capture capacity values comparable to those shown by commercial and previously reported ACs having larger micropore volumes. As the adsorption temperature increased, the CO₂ capture uptake decreased. The sample with a larger micropore volume (chemical activated sample) showed a slightly higher capture capacity than the one shown by the physically activated sample with slightly less percentage of micropore volume. The mesostructural order and CO₂ working capacity of the activated OMCs remained

unchanged after several temperature swing adsorption-desorption cycles at relatively high desorption temperatures (125-200 °C). These results highlight the importance of developing carbon porous materials with a large narrow micropore volume, where the CO₂ adsorption takes place, and with an appropriate mesoporous structure to improve the accessibility of CO₂ to the adsorption sites.

Acknowledgements

This project has received funding from the Research Fund for Coal and Steel (RFCS) of the European Union (EU) under grant agreement No 709741. We also acknowledge Bilbaína de Alquitranes S.A. for providing the creosote used in this work.

References

- (1) Intergovernmental Panel on Climate Change (IPCC), Global warming of 1.5 °C. An IPCC Special Report on the impacts of global warming of 1.5°C, Switzerland, 2018.
- (2) Q. Wang, J. Luo, Z. Zhong, A. Borgna, *Energy Environ. Sci.* 4 (2011) 42-55.
<https://doi.org/10.1039/C0EE00064G>
- (3) R. Cuellar-Franca, A. Azapagic, *J. CO₂ Util.* 9 (2015) 82-102.
<https://doi.org/10.1016/j.jcou.2014.12.001>
- (4) N. Rashidi, S. Yusup, *J. CO₂ Util.* 13 (2016) 1-16.
<https://doi.org/10.1016/j.jcou.2015.11.002>
- (5) S.Y. Lee, S.J. Park, *J. Colloid Interface Sci.* 389 (2013) 230-235.
<https://doi.org/10.1016/j.jcis.2012.09.018>
- (6) C.H. Yu, C.H. Huang, C.S. Tan, *Aerosol and Air Quality Research* 12 (2012) 745-769.
<https://doi.org/10.4209/aaqr.2012.05.0132>
- (7) T.C. Drage, O. Kozynchenko, C. Pevida, M.G. Plaza, F. Rubiera, J.J. Pis, C.E. Snape, S. Tennison, *Energy Procedia* 1 (2009) 599-605. <https://doi.org/10.1016/j.egypro.2009.01.079>
- (8) Marsh, H.; Rodríguez-Reinoso, F.; Activated carbon, Elsevier Sci, 2006.
ISBN: 978-0-08-044463-5, <https://doi.org/10.1016/B978-0-08-044463-5.X5013-4>
- (9) J. Wang, A. Heerwig, M.R. Lohe, M. Oschatz, L. Borchardt, S. Kaskel, *J. Mater. Chem.* 22 (2012) 13911-13913. <https://doi.org/10.1039/C2JM32139D>
- (10) M. Sevilla, A.B. Fuertes, *Energy Environ. Sci.* 4 (2011) 1765-1771.
<https://doi.org/10.1039/C0EE00784F>

- (11) E. García-Díez, S. Schaefer, A. Sanchez-Sanchez, A. Celzard, V. Fierro, M.M. Maroto-Valer, S. Garcia, *ACS Appl. Mater. Interfaces* 11, 40 (2019) 36789-36799. <https://doi.org/10.1021/acsami.9b13247>
- (12) M. Vorokhta, J. Morávková, D. Řimnáčová, R. Pilař, A. Zhigunov, M. Švábová, P. Sazama, *J. CO₂ Util.* 31 (2019) 124-134. <https://doi.org/10.1016/j.jcou.2019.03.001>
- (13) T. Song, J.M. Liao, J. Xiao, L.H. Shen, *New Carbon Mater.* 30(2) (2015) 156-166. [https://doi.org/10.1016/S1872-5805\(15\)60181-0](https://doi.org/10.1016/S1872-5805(15)60181-0)
- (14) M. Li, R. Xiao, *Fuel Process. Tech.* 186 (2019) 35-39. <https://doi.org/10.1016/j.fuproc.2018.12.015>
- (15) Y.C. Lou, S.C. Qi, D.M. Xue, C. Gu, R. Zhou, X.Q. Liu, L.B. Sun, *Chem. Eng. J.* 399 (2020) 125845. <https://doi.org/10.1016/j.cej.2020.125845>
- (16) S. Mane, Y.X. Li, D.M. Xue, X.Q. Liu, L.B. Sun, *Ind. Eng. Chem. Res.* 57 (2018) 12926-12934. <https://doi.org/10.1021/acs.iecr.8b03672>
- (17) D. Zabiegaj, M. Caccia, M.E. Casco, F. Ravera, J. Narciso, *J. of CO₂ Util.* 26 (2018) 36-44. <https://doi.org/10.1016/j.jcou.2018.04.020>
- (18) M.M. Maroto-Valer, Z. Lu, Y. Zhang, Z. Tang, *Waste Management* 28 (2008) 2320-2328. <https://doi.org/10.1016/j.wasman.2007.10.012>
- (19) V. Jimenez, P. Sanchez, J. Valverde, A. Romero, *Mater. Chem. Phys.* 124 (2010) 223-233. <https://doi.org/10.1016/j.matchemphys.2010.06.023>
- (20) W. Zhao, V. Fierro, C. Zlotea, E. Aylon, M.T. Izquierdo, M. Latroche, A. Celzard, *Int. J. Hydrogen Energ.* 36 (2011) 18, 11746-11751. <https://doi.org/10.1016/j.ijhydene.2011.05.181>

- (21) F. Dong, C. Liu, M. Wu, J. Guo, K. Li, J. Qiao, *ACS Sustain. Chem. Eng.* 7, 9 (2019) 8587-8596. <https://doi.org/10.1021/acssuschemeng.9b00373>
- (22) J. Serafin, U. Narkiewicz, A.W. Morawski, R.J. Wróbel, B. Michalkiewicz, *J. CO₂ Util.* 18 (2017) 73-79. <https://doi.org/10.1016/j.jcou.2017.01.006>
- (23) A.L. Yaumi, M.Z. Abu Bakar, B.H. Hameed, *Energy* 124 (2017) 461-480. <https://doi.org/10.1016/j.energy.2017.02.053>
- (24) M. Nowrouzi, H. Younesi, N. Bahramifar, *Fuel* 223 (2018) 99-114. <https://doi.org/10.1016/j.fuel.2018.03.035>
- (25) S.C. Qi, Y. Liu, A.Z. Peng, D.M. Xue, X. Liu, X.Q. Liu, L.B. Sun, *Chem. Eng. J.* 361 (2019) 945-952. <https://doi.org/10.1016/j.cej.2018.12.167>
- (26) A.B. Fadhil, A.I. Ahmed, H.A. Salih, *Fuel* 187 (2017) 435-445. <https://doi.org/10.1016/j.fuel.2016.09.064>
- (27) A. Jeder, A. Sanchez-Sanchez, P. Gadonneix, E. Masson, A. Ouederni, A. Celzard, V. Fierro, *Environ. Sci. Pollut. Res. Int.* 25, 2 (2018) 1497-1507. <https://doi.org/10.1007/s11356-017-0366-7>
- (28) S. Taher, A. Sanchez-Sanchez, P. Gadonneix, J. Jagiello, M. Seffen, H. Sammouda, A. Celzard, V. Fierro, *Indus. Crops Prod.* 115 (2018) 146-157. <https://doi.org/10.1016/j.indcrop.2018.02.005>
- (29) S. Schaefer, G. Muñiz, M.T. Izquierdo, S. Mathieu, M.L. Ballinas-Casarrubias, G. González-Sánchez, A. Celzard, V. Fierro, *Int. J. Hydrogen Energy* 42, 16 (2017) 11534-11540. <https://doi.org/10.1016/j.ijhydene.2017.02.043>
- (30) D. Qiu, C. Kang, M. Li, J. Wei, Z. Hou, F. Wang, R. Yang, *Carbon* 162 (2020) 595-603. <https://doi.org/10.1016/j.carbon.2020.02.083>

- (31) W.T. Tsai, C.Y. Chang, S.L. Lee, *Carbon* 35 (1997) 1198-1200.
[https://doi.org/10.1016/s0008-6223\(97\)84654-4](https://doi.org/10.1016/s0008-6223(97)84654-4)
- (32) R. Ryoo, S.H. Joo, M. Kruk, M. Jaroniec, B.R. Ryoo, S.H. Joo, M. Kruk, M. Jaroniec, *Adv. Mater.* 13 (2001) 677–681.
[https://doi.org/10.1002/1521-4095\(200105\)13:9<677::AID-ADMA677>3.0.CO;2-C](https://doi.org/10.1002/1521-4095(200105)13:9<677::AID-ADMA677>3.0.CO;2-C)
- (33) J. Lee, J. Kim, T. Hyeon, *Adv. Mater.* 18 (2006) 2073–2094.
<https://doi.org/10.1002/adma.200501576>
- (34) Y. Xia, Z. Yang, R. Mokaya, R.; Templated Porous Carbon Materials: Recent Developments, in: D.W. Bruce, D. O'Hare, R.I. Walton (Eds.), *Porous Mater.*, John Wiley & Sons, Ltd, Chichester, UK, 2011: pp. 217–264. <https://doi.org/10.1002/9780470711385.ch4>
- (35) M. Enterría, F. Suárez-García, A. Martínez-Alonso, J.M.D. Tascón, *Microporous Mesoporous Mater.* 151 (2012) 390–396. <https://doi.org/10.1016/j.micromeso.2011.10.004>
- (36) A. Castro-Muñiz, S. Lorenzo-Fierro, A. Martínez-Alonso, J.M.D. Tascón, V. Fierro, F. Suárez-García, J.I. Paredes, *Fuel Process. Technol.* 196 (2019) 106152.
<https://doi.org/10.1016/j.fuproc.2019.106152>
- (37) K.B. Lee, S. Sircar, *AIChE J.* 54 (2008) 2293-2302. <https://doi.org/10.1002/aic.11531>
- (38) S. Choi, J.H. Drese, C.W. Jones, *ChemSusChem.* 2 (2009) 796-854.
<https://doi.org/10.1002/cssc.200900036>
- (39) D. Zhao, J. Feng, Q. Huo, N. Melosh, G.H. Fredrickson, B.F. Chmelka, G.D. Stucky, *Science* 279 (1998) 548-552. <https://doi.org/10.1126/science.279.5350.548>
- (40) T.W. Kim, I.S. Park, R. Ryoo, *Angew. Chemie Int. Ed.* 42 (2003) 4375–4379.
<https://doi.org/10.1002/ange.200352224>

- (41) A.F. Léonard, A. Castro-Muñiz, F. Suárez-García, N. Job, J.I. Paredes, *Microporous Mesoporous Mater.* (2020) 110417. <https://doi.org/10.1016/j.micromeso.2020.110417>
- (42) S. Sjöberg, S. Sjöberg, *J. Non. Cryst. Solids.* 196 (1996) 51–57.
[https://doi.org/10.1016/0022-3093\(95\)00562-5](https://doi.org/10.1016/0022-3093(95)00562-5)
- (43) G. Alexander, W. Heston, R. Iler, *J. Phys. Chem.* 58 (1954) 453–455.
<https://doi.org/10.1021/j150516a002>
- (44) M. Enterría, F. Suárez-García, A. Martínez-Alonso, J.M.D. Tascón, *Microporous Mesoporous Mater.* 151 (2012) 390-396. <https://doi.org/10.1016/j.micromeso.2011.10.004>
- (45) M. Enterría, F. Suárez-García, A. Martínez-Alonso, J.M.D. Tascón, *Carbon* 50 (2012), 3826-3835. <https://doi.org/10.1016/j.carbon.2012.04.024>
- (46) S. Brunauer, P. Emmet, E. Teller, *J. Am. Chem. Soc.* 60, 2 (1938) 309-319.
<https://doi.org/10.1021/ja01269a023>
- (47) N. Dubinin, *Carbon* 27(3) (1989) 457-467. [https://doi.org/10.1016/0008-6223\(89\)90078-X](https://doi.org/10.1016/0008-6223(89)90078-X)
- (48) A.V. Neimark, Y. Lin, P.I. Ravikovitch, M. Thommes, *Carbon* 47 (2009) 1617-1628.
<https://doi.org/10.1016/j.carbon.2009.01.050>
- (49) D. Cazorla-Amorós, J. Alcañiz-Monge, M.A. de la Casa-Lillo, A. Linares-Solano, *Langmuir*, 14 (1998) 4569-4596. doi: <https://doi.org/10.1021/la980198p>
- (50) M. Thommes, K. Kaneko, A.V. Neimark, J.P. Oliver, F. Rodriguez-Reinoso, J. Rouquerol, K.S. Sing, *Pure Appl. Chem.* 9-10, 87 (2015) 1051-1069.
<https://doi.org/10.1515/pac-2014-1117>
- (51) F. Rouquerol, J. Rouquerol, K. Sing, *Adsorption by powders and porous solids.* Academic Press, London, **1999**. ISBN: 978-0-12-598920-6,

<https://doi.org/10.1016/B978-0-12-598920-6.X5000-3>

(52) M. Thommes, *Chemie Ingenieur Technik* 82 (2010) 1059-1073.

<https://doi.org/10.1002/cite.201000064>

(53) J. Jagiello, M. Thommes, *Carbon* 42 (2004) 1227–1232.

<https://doi.org/10.1016/j.carbon.2004.01.022>

(54) A. Castro-Muñiz, S. Lorenzo-Fierro, A. Martínez-Alonso, J.M.D. Tascón, V. Fierro, F. Suárez-García, J.I. Paredes, *Fuel Process. Technol.* 196 (2019) 106152.

<https://doi.org/10.1016/j.fuproc.2019.106152>

(55) Y. Zhai, Y. Wan, Y. Cheng, Y. Shi, F. Zhang, B. Tu, D. Zhao, *J. Porous Mater.* 15 (2008) 601-611. <https://doi.org/10.1007/s10934-007-9139-x>

(56) R. Ryoo, S.H. Joo, M. Kruk, M. Jaroniec, *Adv. Mater.* 13 (2001) 677-681.

[https://doi.org/10.1002/1521-4095\(200105\)13:9<677::AID-ADMA677>3.0.CO;2-C](https://doi.org/10.1002/1521-4095(200105)13:9<677::AID-ADMA677>3.0.CO;2-C)

(57) D.J. Tao, F.F. Mao, J.J. Luo, Y. Zhou, Z.M. Li, L. Zhang, *Mat. Today Com.* 22 (2020)

100849. <https://doi.org/10.1016/j.mtcomm.2019.100849>

(58) S.M.W. Wilson, D.A. Kennedy, F.H. Tezel, *Sep. and Purification Techn.* 236 (2020) 116268.

(59) A.A. Abd, S.Z. Naji, A.S. Hashim, M.R. Othman, *J. of Environm. Chem. Eng.* 8 (2020)

104142. <https://doi.org/10.1016/j.jece.2020.104142>

(60) V. Safarifard, S. Rodríguez-Hermida, V. Guillerm, I. Imaz, M. Bigdeli, A.A. Tehrani, J. Juanhuix, A. Morsali, M.E. Casco, J. Silvestre-Albero, E.V. Ramos-Fernandez, D. Maspoch, *Cryst. Growth Des.* 16, 10 (2016) 6016-6023. <https://doi.org/10.1021/acs.cgd.6b01054>

(61) D. Zabiegaj, M. Caccia, M.E. Casco, F. Ravera, J. Narciso, *J. of CO₂ Util* 26 (2018) 36-44. <https://doi.org/10.1016/j.jcou.2018.04.020>

- (62) A. Sánchez-Sánchez, F. Suárez-García, A. Martínez-Alonso, J.M.D. Tascón, *ACS Appl. Mater. Interfaces* 6, 23 (2014) 21237-21247. <https://doi.org/10.1021/am506176e>
- (63) A. Arenillas, K.M. Smith, T.C. Drage, C.E. Snape, *Fuel* 84 (2005) 2204-2210. <https://doi.org/10.1016/j.fuel.2005.04.003>
- (64) M.G. Plaza, S. García, F. Rubiera, J.J. Pis, C. Pevida, *Chem. Eng. J.* 163 (2010) 41-47. <https://doi.org/10.1016/j.cej.2010.07.030>
- (65) E. Qezelsefloo, S. Khalili, M. Jahanshahi, M. Peyravi, *Mat. Chem. and Physics* 239 (2020) 122304. <https://doi.org/10.1016/j.matchemphys.2019.122304>

Table list

Table 1. Porous textural parameters derived from the N₂ adsorption isotherms at -196 °C and the CO₂ adsorption isotherms at 0 °C of the original carbon and the chemical and physical activated carbons.

Sample name	N ₂ adsorption					CO ₂ adsorption
	S_{BET} (m ² /g)	V_T (cm ³ /g)	V_{DR, N_2} (cm ³ /g)	V_{mp} (cm ³ /g)	% V_{mp}	V_{DR, CO_2} (cm ³ /g)
OMCreo	937	1.08	0.34	0.74	69	0.18
OMCreo CA 4:1 650	973	0.88	0.36	0.53	60	0.20
OMCreo CA 4:1 750	1252	0.90	0.47	0.43	48	0.23
OMCreo CA 4:1 850	1586	1.12	0.62	0.50	45	0.29
OMCreo CA 3:1 850	1232	1.17	0.44	0.73	62	0.24
OMCreo CA 2:1 850	1030	1.02	0.38	0.64	62	0.20
OMCreo CA 1:1 850	962	1.04	0.35	0.69	66	0.18
OMCreo PAt 3%	1050	1.12	0.38	0.74	66	0.21
OMCreo PAt 48%	1571	1.35	0.59	0.76	56	0.26
OMCreo PAc 15%	1144	1.26	0.41	0.85	67	0.27
OMCreo PAc 45%	1701	1.08	0.34	0.74	69	0.26

Table 1. Porous textural parameters derived from the N₂ adsorption isotherms at -196 °C and the CO₂ adsorption isotherms at 0 °C of the original carbon and the chemical and physical activated carbons.

Figure list

Scheme 1. Schematic of the preparation of ordered mesoporous carbons via hard template method.

Figure 1. N₂ adsorption isotherms at -196 °C (a), CO₂ adsorption isotherms at 0 °C (b) and PSDs obtained by applying the NLDFT method to the N₂ (c) and CO₂ (d) adsorption isotherms for the samples prepared with a KOH:Carbon ratio of 4:1 and at different activation temperatures.

Figure 2. N₂ adsorption isotherms at -196 °C (a), CO₂ adsorption isotherms at 0 °C (b) and PSDs obtained by applying the NLDFT method to the N₂ (c) and CO₂ (d) adsorption isotherms for the samples prepared at 850 °C with different KOH:Carbon ratios.

Figure 3. N₂ adsorption isotherms at -196 °C (a), CO₂ adsorption isotherms at 0 °C (b) and PSDs obtained by applying the NLDFT method to the N₂ (c) and CO₂ (d) adsorption isotherms for the physically activated samples.

Figure 4. Low-angle XRD patterns of the samples prepared with a KOH:Carbon ratio of 4:1 and at different activation temperatures (a), prepared at 850 °C with different KOH:Carbon ratios (b) and by physical activation (c).

Figure 5. TEM micrographs of OMCreo CA 1:1 850 (a), OMCreo CA 4:1 850 (b), OMCreo PAc 45% (c) and OMCreo PAt 48% (d).

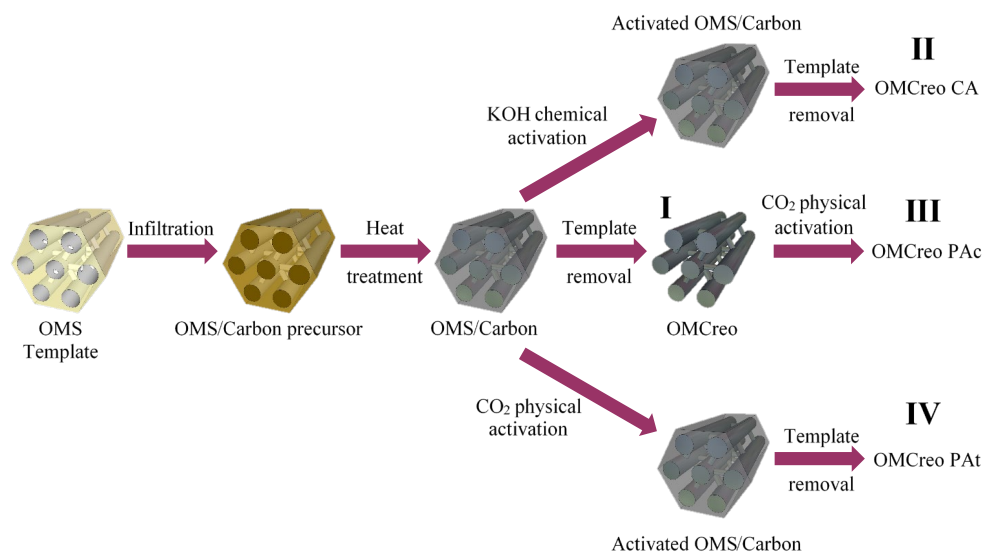
Figure 6. CO₂ capture capacity (mmol/g AOMC) for prepared activated carbons. (Black for OMCreo not activated sample, blue for chemically activated samples, and red for physically activated).

Figure 7. CO₂ capture capacity of samples OMCreo CA 4:1 850 and OMCreo PAt 48% as a function of adsorption temperature. (Blue for OMCreo CA 4:1 850 and red for OMCreo PAt 48%).

Figure 8. CO₂ capture capacities of samples OMCreo CA 4:1 850 and OMCreo PAt 48% as a function of the CO₂ partial pressure in the adsorption process at 25°C. (Blue for OMCreo CA 4:1 850 and red for OMCreo PAt 48%).

Figure 9. Cycles adsorption-desorption; variation of weight at 25 °C and desorption at 200 °C. OMCreo CA 4:1 850 (a) OMCreo PAt 48% (b).

Figure 10. CO₂ working capacities at different desorption temperatures (125 – 200 °C) for the OMCreo CA 4:1 850 (a) and OMCreo PAt 48% (b).



Scheme 1. Schematic of the preparation of ordered mesoporous carbons via hard template method.

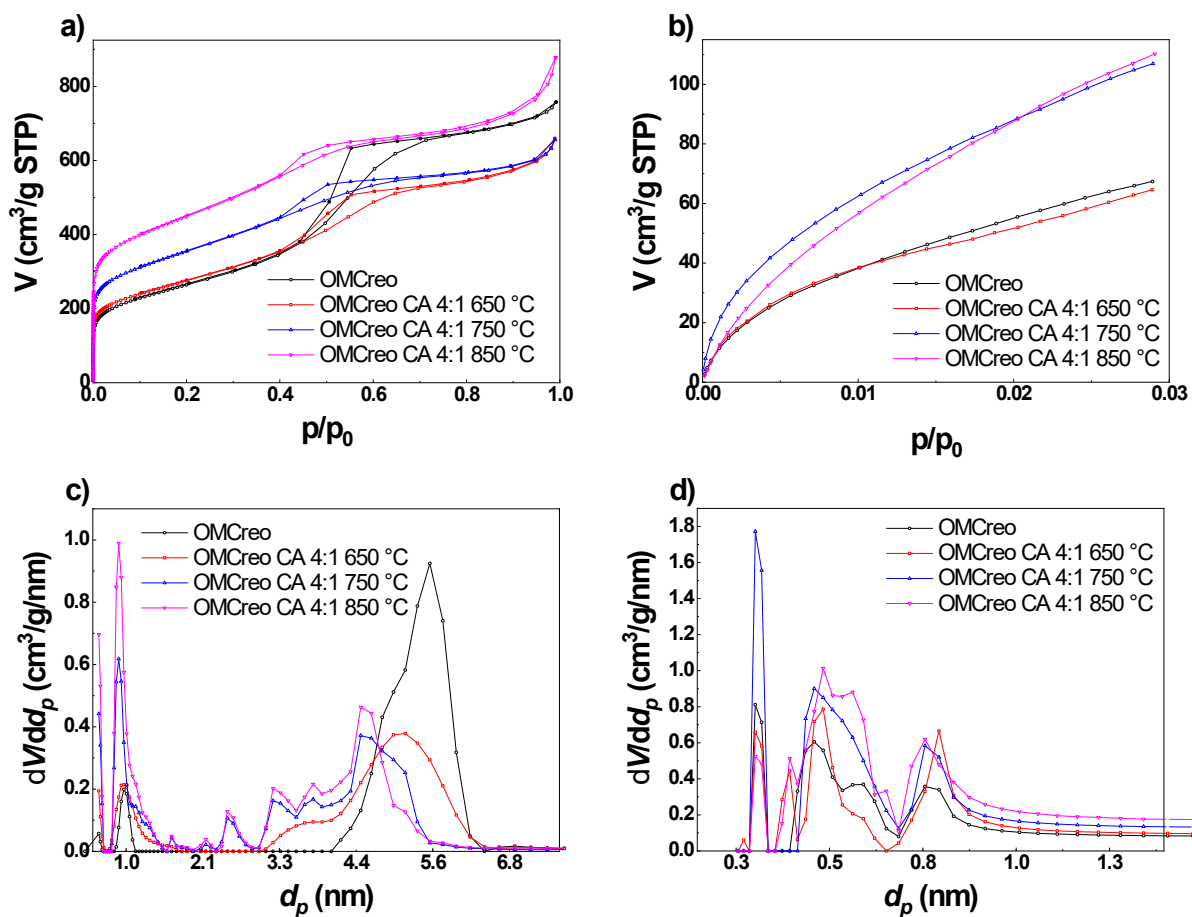


Figure 1. N₂ adsorption isotherms at -196 °C (a), CO₂ adsorption isotherms at 0 °C (b) and PSDs obtained by applying the NLDFIT method to the N₂ (c) and CO₂ (d) adsorption isotherms for the samples prepared with a KOH:Carbon ratio of 4:1 and at different activation temperatures.

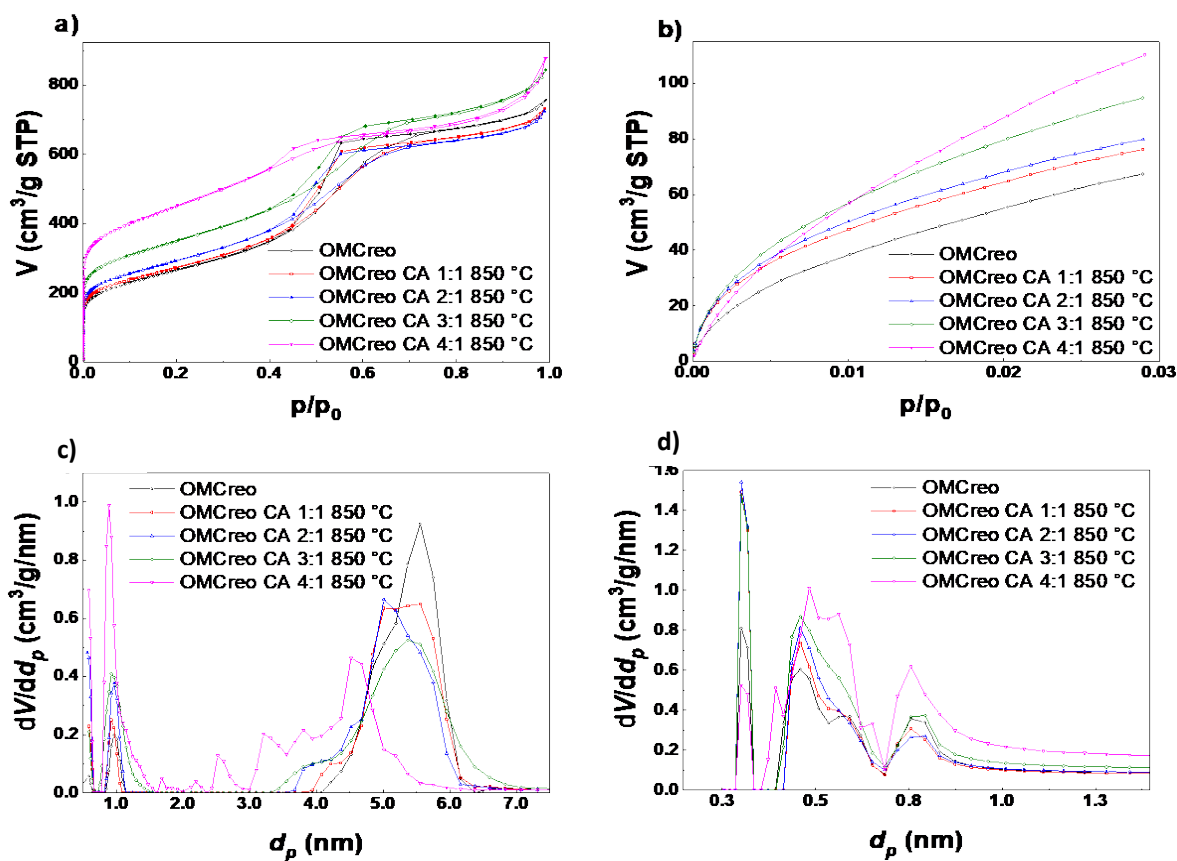


Figure 2. N₂ adsorption isotherms at -196 °C (a), CO₂ adsorption isotherms at 0 °C (b) and PSDs obtained by applying the NLDFT method to the N₂ (c) and CO₂ (d) adsorption isotherms for the samples prepared at 850 °C with different KOH:Carbon ratios.

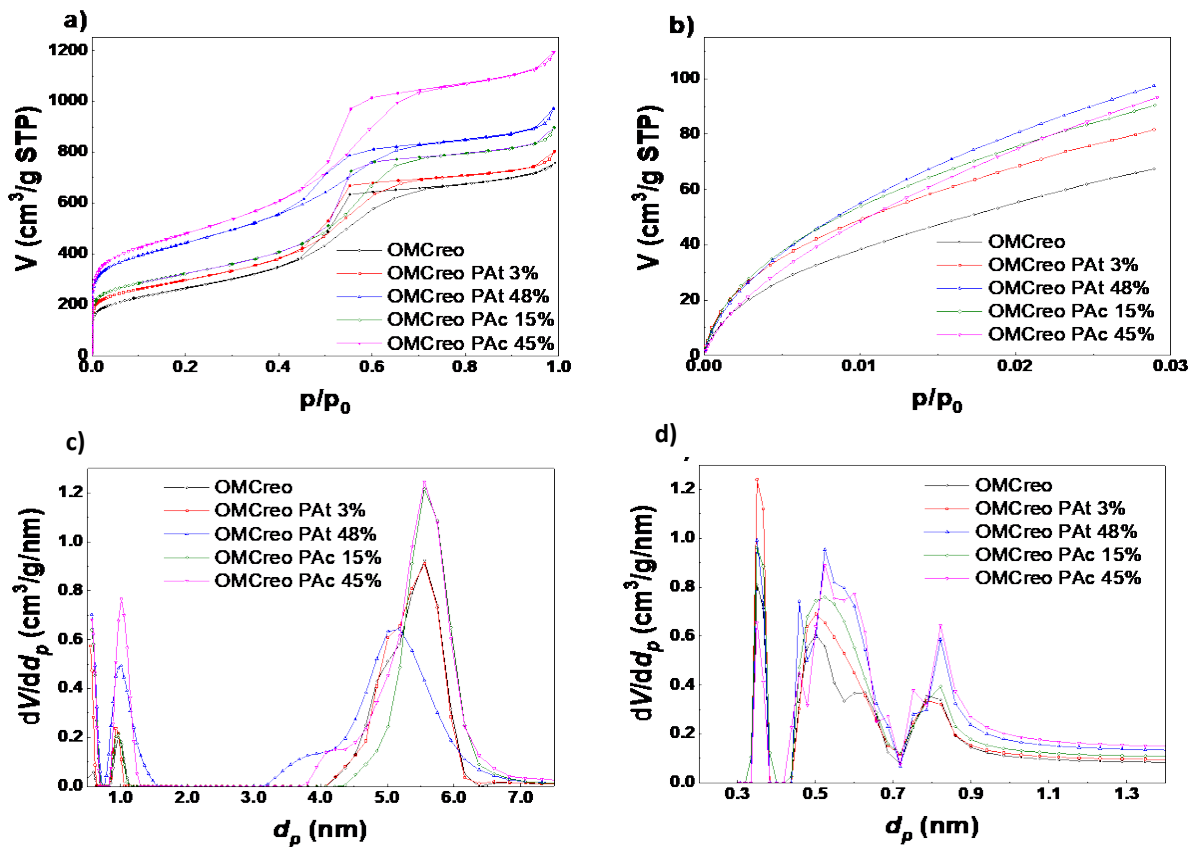


Figure 3. N₂ adsorption isotherms at -196 °C), CO₂ adsorption isotherms at 0 °C (b) and PSDs obtained by applying the NLDFIT method to the N₂ (c) and CO₂ (d) adsorption isotherms for the physically activated samples.

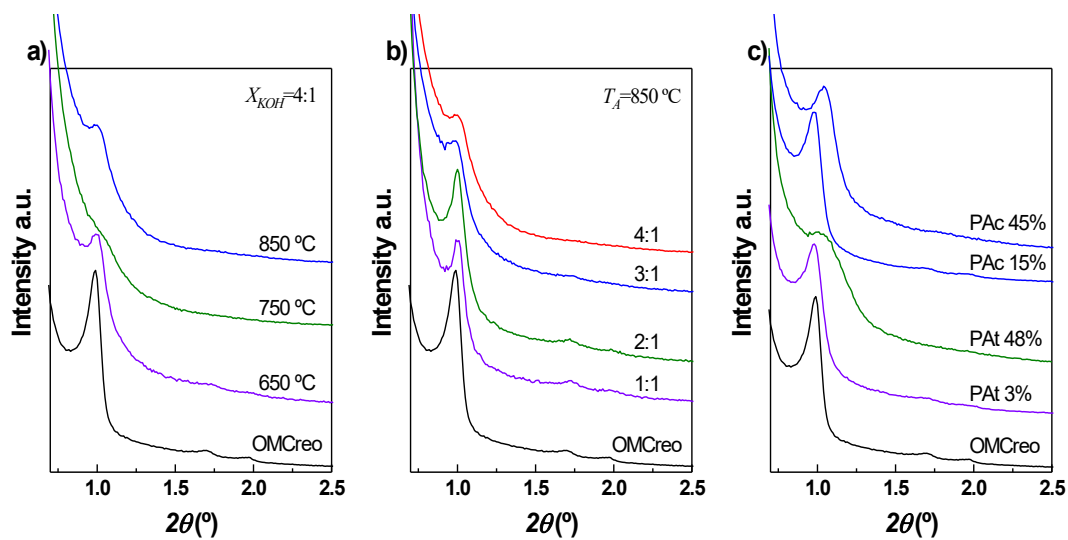


Figure 4. Low-angle XRD patterns of the samples prepared with a KOH:Carbon ratio of 4:1 and at different activation temperatures (a), prepared at 850 °C with different KOH:Carbon ratios (b) and by physical activation (c).

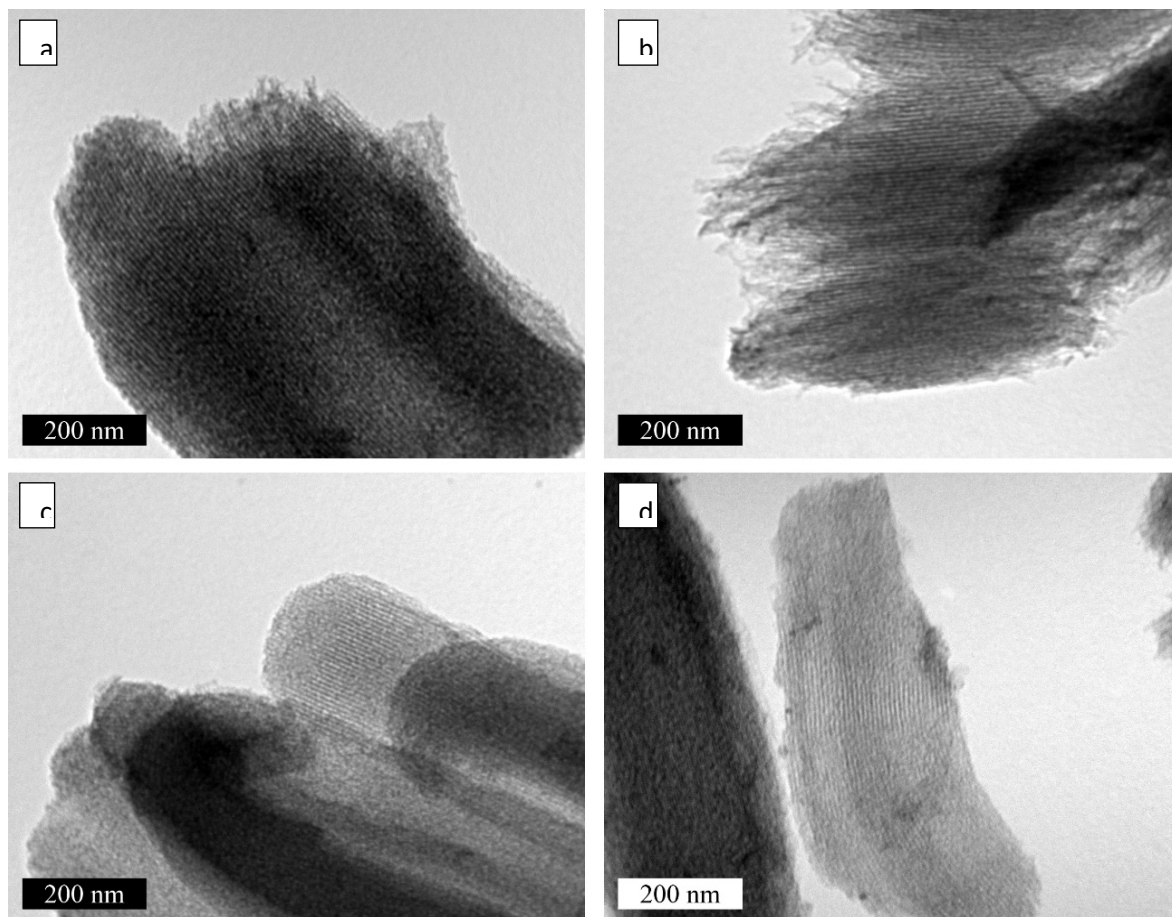


Figure 5. TEM micrographs of OMCreo CA 1:1 850 (a), OMCreo CA 4:1 850 (b), OMCreo PAc 45% (c) and OMCreo PAt 48% (d).

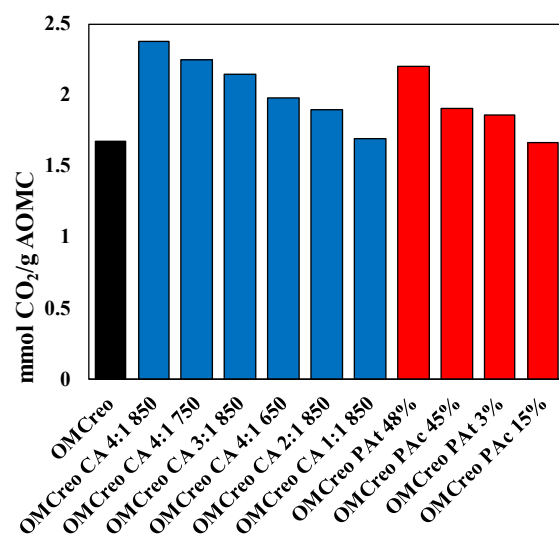


Figure 6. CO₂ capture capacity (mmol/g AOMC) for prepared activated carbons. (Black for OMCreo not activated sample, blue for chemically activated samples, and red for physically activated).

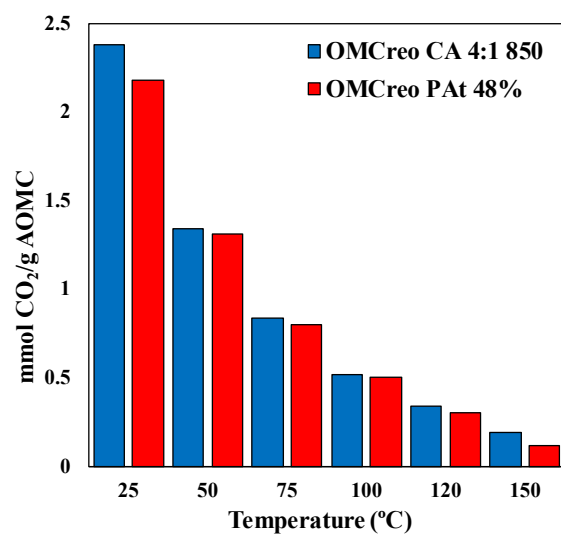


Figure 7. CO₂ capture capacity of samples OMCreo CA 4:1 850 and OMCreo PAt 48% as a function of adsorption temperature. (Blue for OMCreo CA 4:1 850 and red for OMCreo PAt 48%).

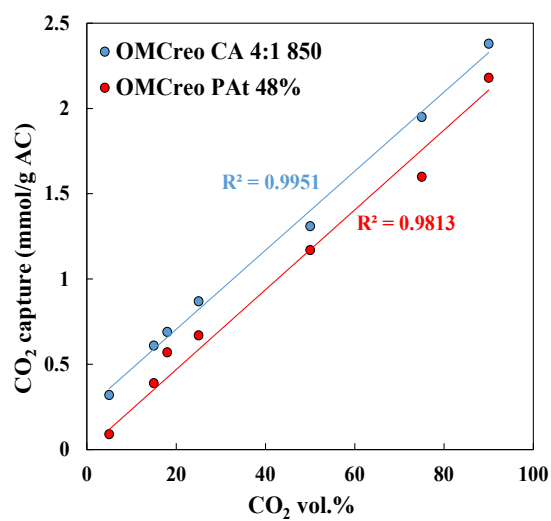


Figure 8. CO₂ capture capacities of samples OMCreo CA 4:1 850 and OMCreo PAt 48% as a function of the CO₂ partial pressure in the adsorption process at 25°C. (Blue for OMCreo CA 4:1 850 and red for OMCreo PAt 48%).

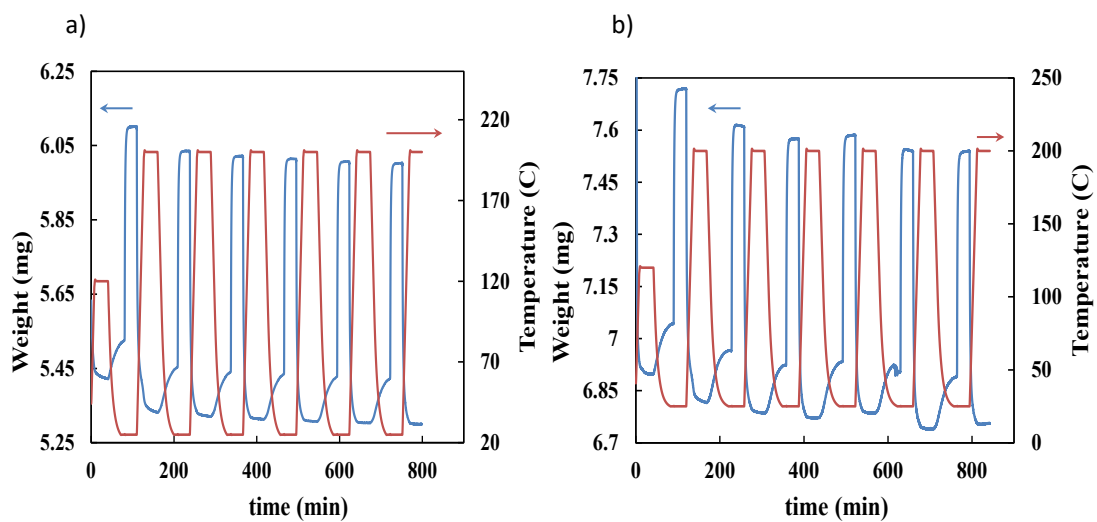


Figure 9. Cycles adsorption-desorption; variation of weight at 25 °C and desorption at 200 °C.

OMCreo CA 4:1 850 (a) OMCreo PAt 48% (b).

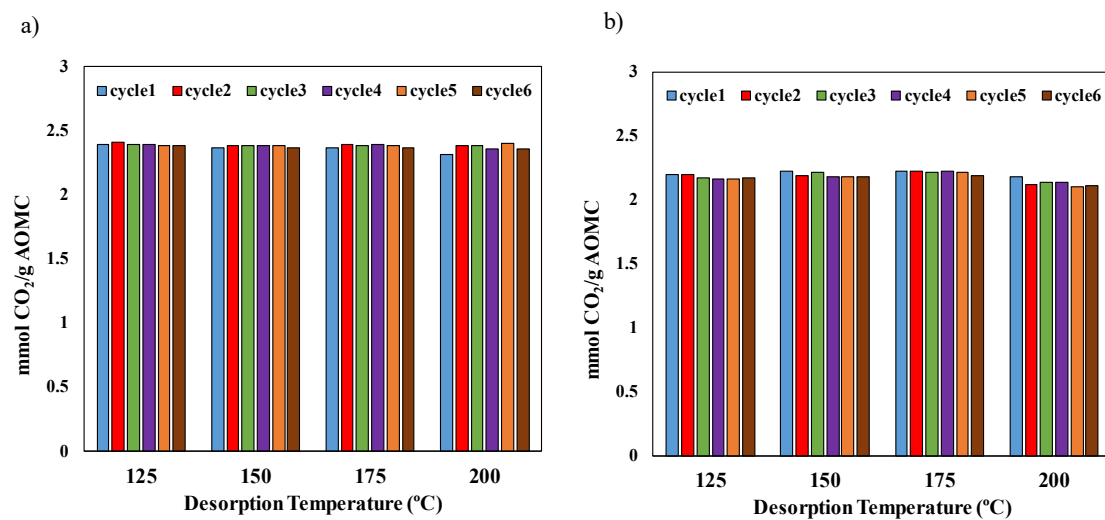


Figure 10. CO₂ working capacities at different desorption temperatures (125 – 200 °C) for the OMCreo CA 4:1 850 (a) and OMCreo PAt 48% (b).